J. Fluid Mech. (1995), *vol.* 293, *pp.* 379–403

A new model to determine dynamic surface tension and elongational viscosity using oscillating jet measurements

By S.E. BECHTEL[1], J.A. COOPER[2], M.G. FOREST[3], N.A. PETERSSON[4], D.L. REICHARD[2], A. SALEH[5] AND V. VENKATARAMANAN[1]

[1] Department of Engineering Mechanics, The Ohio State University, Columbus, OH 43210, USA

[2] US Department of Agriculture, Agricultural Research Service, Wooster, OH 44691, USA

[3] Department of Mathematics, The Ohio State University, Columbus, OH 43210, USA

[4] Center for Nonlinear Studies, Los Alamos National Laboratory, Los Alamos, NM 87545, USA

[5] Department of Civil Engineering, The Ohio State University, Columbus, OH 43210, USA

(Received 18 October 1994 and in revised form 3 February 1995)

We present an integro-differential equation model which, combined with experimental measurements of an oscillating free surface jet, calculates dynamic surface tension and elongational viscosity of a fluid. Our model builds upon previous models due to Rayleigh and Bohr in that it self-consistently incorporates the effects of viscosity and gravity. Further, surface tension and viscosity are allowed to be non-constant. The principal result of this paper is a technique for the measurement of surface tension of newly forming surfaces on the millisecond timescale relevant for agricultural spray mixtures. Coincidentally, our model independently yields the elongational viscosity of the fluid, although our present experimental apparatus limits the accuracy of measurement of this material property.

In this paper we take measurements from physical jet experiments and implement our inverse model to deduce these material properties. The model is first benchmarked against standard techniques on a well-characterized fluid with constant surface tension and Newtonian viscosity. We then apply our method to an agricultural spray mixture, with non-constant surface tension and non-Newtonian rheology. We measure (i) the rapid decay of surface tension from the newly formed surface (aged less than a millisecond) to the much lower equilibrium value, and (ii) the rate dependence of elongational viscosity.

1. The oscillating jet phenomenon, and its application for the determination of dynamic surface tension

Measurements of oscillating free surface jets have long been used, together with analytical models, to determine the surface tension of fluids. The oscillating jet phenomenon can be described as follows. When a fluid issues from an elliptical orifice of moderate aspect ratio (say 2.0 or less), the initial elliptical cross-section of the jet deforms downstream towards a circular shape, then overshoots the circle and

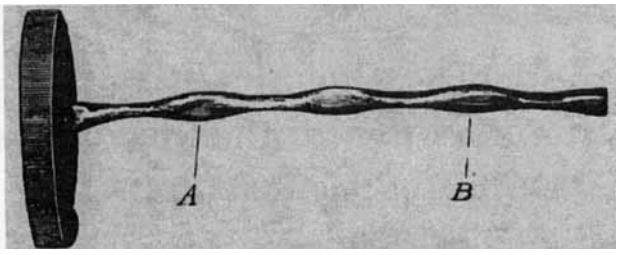

FIGURE 1. The oscillating jet phenomenon from Rayleigh (1890).

returns to become essentially elliptical, but with major axis perpendicular to that of the orifice. Further down the jet the cross-section again approximates an ellipse, this time with major axis parallel to that of the orifice (figure 1). This oscillation between two perpendicular directions continues until either the oscillations are damped or the jet breaks up due to capillary instability.

An oscillating jet executes a vibration that is stationary for the length of the jet before breakup occurs. This stationary behaviour is key to the use of the oscillating jet as an experimental technique, as it allows the accurate measurement of jet features such as wavelength and amplitude. The oscillating jet is a liquid/gas system in which a new free surface is created constantly. In agricultural mixtures, the surface tension of the interface may decrease by a factor of two or more from the initial exit to the equilibrium or static value. In oscillating jet experiments, the age of the surface can be controlled by selecting the locations where measurements are made, the orifice size and the flow rate. Given a relation between the surface tension and the wavelength of the jet, the surface tension of the newly formed surface (on the controlled timescale) is deduced through the standard inverse method from experimental measurements. In our inverse method, this relation is given by a nonlinear integro-differential equation for the steady free surface, with material properties such as surface tension and elongational viscosity appearing as coefficients in the equation.

It is recognized that constitutive relations and material properties are often strongly flow and flow-rate dependent. An important advantage of the oscillating jet technique is that many practical applications such as spray formation, fibre spinning, and extrusion processes involve fundamentally similar flow behaviour – the forcing of material in a liquid state through an orifice and the creation of a free surface in air or some other gas. Thus the oscillating jet technique determines material properties such as dynamic surface tension in a flow which closely approximates the intended application. Furthermore, as noted above one can tune the experiments to assess the dynamic surface tension on the timescale relevant for a specific process. For example, in agricultural sprays one seeks the dynamic surface tension on the timescale of drop formation (which happens to be milliseconds). To our knowledge the oscillating jet is the only technique that allows surface tension measurements on the very short timescales relevant for many manufacturing, solidification, and agricultural processes. In these applications, important free surface phenomena occur well before the surface tension value has stabilized to a static, equilibrium value. As we show here, our technique predicts surface tension values for a particular agricultural spray mixture at 0.6 ms and 1.8 ms which are 2.58 and 1.96 times the equilibrium surface tension measured by the DuNouy ring, respectively. (Zhang, Harris & Basaran (1994) describe a recently developed growing drop technique that can determine the surface tension of an interface with a surface age as low as 20 ms.)

An oscillating free surface jet can also be exploited to determine elongational viscosity. The flow in an oscillating free surface jet is elongational to leading order, in an asymptotic sense made explicit in §4, equation (4.8). Thus, any viscous effects are indicative of elongational rather than shear viscosity. For Newtonian fluids, we use the Trouton relation to deduce shear viscosity and compare against tabulated values obtained using standard shear viscometers. For non-Newtonian fluids, for which the shear and elongational viscosities are unrelated, our methods yield elongational viscosity (in the transverse cross-section of the flow). The effect of viscosity in experiments and in the model is to lessen the amplitude of spatial oscillation over each successive wavelength downstream; we exploit this behaviour in our inverse code which uses experimental measurements of decreasing amplitude of the jet oscillation to deduce the elongational viscosity of the fluid. This facility of the oscillating jet technique has not been previously exploited to our knowledge, and should be useful for material characterization of non-Newtonian fluids such as molten polymers.

2. The three-dimensional boundary value problem

We assume that the jet is flowing in the direction of gravity. A fixed rectangular Cartesian coordinate system x_1, x_2, x_3 with unit vectors $\boldsymbol{e}_1, \boldsymbol{e}_2, \boldsymbol{e}_3$, is adopted with the x_3 axis along the centreline of the jet and increasing in the direction of gravity. The fluid is assumed to be incompressible and generalized Newtonian, so that its Cauchy stress is given by

$$\boldsymbol{T} = \tfrac{2}{3}\eta \boldsymbol{D} - p\boldsymbol{I}, \tag{2.1}$$

where η is the elongational viscosity (not necessarily a constant), $\boldsymbol{D}$ is the symmetric part of the velocity gradient, and p is the constraint pressure. In Cartesian component notation, using indicial notation and the summation convention, the Cauchy stress is

$$T_{ij} = \tfrac{1}{3}\eta(v_{i,j} + v_{j,i}) - p\delta_{ij}, \tag{2.2}$$

where v_1, v_2, and v_3 are the velocity components in the x_1, x_2, and x_3 directions, respectively, and δ_{ij} is the Kronecker symbol. The three-dimensional field equations for the fluid are the incompressibility constraint

$$\nabla \cdot \boldsymbol{v} = v_{i,i} = 0, \tag{2.3}$$

and the three components of the momentum equation,

$$T_{ij,j} + \delta_{i3}\rho g = \rho(v_{i,t} + v_j v_{i,j}), \tag{2.4}$$

where ρ is the density of the fluid (assumed constant) and g is the acceleration due to gravity.

The kinematic free surface boundary condition on the free surface is

$$f_{,t} + v_i f_{,i} = 0, \tag{2.5}$$

where

$$f(x_1, x_2, x_3, t) = 0 \tag{2.6}$$

is the equation of the free surface. We model surface tension with the kinetic (or traction) free surface boundary condition (Edwards, Brenner & Wasan 1991; Milliken, Stone & Leal 1993),

$$[\boldsymbol{T}_a - \boldsymbol{T}]\boldsymbol{n} = \sigma\kappa\boldsymbol{n} + \nabla_s\sigma, \tag{2.7}$$

where $\boldsymbol{T}$ and $\boldsymbol{T}_a$ are the stress tensors in the fluid and the ambient gas, respectively,

$\boldsymbol{n}$ is the outward unit normal to the free surface, and κ is the mean curvature of the free surface. The surface tension σ is a function of position on the free surface, i.e. $\sigma = \sigma(x_s, y_s, z)$, where the subscripts indicate that the point is on the surface, and ∇_s refers to the gradient operator on the free surface defined by (Stone & Leal 1990)

$$\nabla_s = [\boldsymbol{I} - \boldsymbol{n} \otimes \boldsymbol{n}]\nabla. \tag{2.8}$$

We also assume that $\boldsymbol{T}_a$ is given by

$$\boldsymbol{T}_a = -p_a \boldsymbol{n}, \tag{2.9}$$

where p_a is a specified constant pressure exerted by the ambient atmosphere.

3. Previous oscillating jet models

The direct analytical model for an oscillating free surface jet with elliptical cross-section ideally consists of the three-dimensional boundary value problem formulated in the last section. The inverse analytical model likewise ideally consists of posing properties of steady solutions, acquired from physical measurements of an actual jet, from which the surface tension coefficient and perhaps other material properties are deduced. However, it is impractical to perform such an analysis directly on the three-dimensional boundary value problem (b.v.p.) of the previous section, since adequate three-dimensional simulations are prohibitively expensive and slow. In fact, accurate numerical simulations for surface-tension-dominated flows remain an area of intense research (Chang *et al.* 1995; Hou, Lowengrub & Shelley 1994; Pozrikidis 1992; Basaran 1992; Hou, Lowengrub & Krasny 1991; Mansour & Lundgren 1990).

Alternatively, one may place simplifying assumptions on the full three-dimensional b.v.p. to make the problem computationally tractable. Lord Rayleigh (1879, 1890) provided the first development of a simplified analytical model which together with experimental measurements of a nearly axisymmetric, oscillating jet could be used for the determination of the dynamic surface tension of an inviscid liquid/air interface. Limitations and lack of practical viability of Rayleigh's model were recognized by Pedersen (1907). Bohr (1909) proposed an improved model that removes some of the limitations of Rayleigh's theory. In his upgraded model, viscosity corrections and adjustments due to non-circular jet cross-sections augment Rayleigh's formula. Bohr's model is still the state-of-the-art one for determining dynamic surface tension in combination with measurements of oscillating jets. Each of these classical inverse models consists of an explicit formula for surface tension which is applied in conjunction with specified experimental measurements.

3.1. *Rayleigh's model*

Rayleigh's (1879) assumptions are the following.

(*a*) Gravity is neglected.

(*b*) The surface tension and density are constant over the axial length in which measurements are taken.

(*c*) Apart from a global, uniform translation, the jet flow occurs only in the two transverse directions. This assumption of a uniform axial velocity presupposes that gravity is neglected (assumption (*a*)) and surface tension is constant (assumption (*b*)).

(*d*) The fluid is inviscid.

(*e*) The departure of the free surface cross-section from a circle is small.

Rayleigh assumes a cylindrical free surface of the form

$$r(\theta, t) = a_0(1 + \delta \cos n\theta \cos \omega t + O(\delta^2)). \tag{3.1}$$

In the case $n = 2$, which for small δ approximates an elliptical surface, the linearized frequency (ω) of oscillation is

$$\omega^2 = 6\sigma/\rho a_0^3. \tag{3.2}$$

From assumption (*c*) one sees that Rayleigh solved a problem related to that shown in figure 1 of a jet issuing from an elliptical orifice. He then translates the two-dimensional oscillating cylinder solution to the solution of a jet issuing from an elliptic orifice by assuming that each jet material cross-section in figure 1 oscillates within its plane according to the two-dimensional solution, while translating with a constant velocity v. Therefore a period $T = 2\pi/\omega$ of the temporal oscillation of the material cross-section happens over a wavelength

$$\lambda = v\,T = 2\pi v/\omega, \tag{3.3}$$

so that, combining (3.2) and (3.3), surface tension σ can be deduced from the measured wavelength λ by

$$\sigma = 2\pi^2 v^2 \rho a_0^3/3\lambda^2. \tag{3.4}$$

3.2. *Bohr's model*

Bohr (1909) recognized the practical limitations of Rayleigh's assumptions (*d*) and (*e*): the inviscid assumption is unrealistic for many liquids and infinitesimal departures from a circular cross-section cannot be measured with a sufficient degree of accuracy.

Bohr offered three improvements to Rayleigh's model.

(i) The effect of viscosity on the period of oscillation of the jet is accounted for by generalizing Rayleigh's linearized analysis (3.1)–(3.4) to a weakly Newtonian viscous fluid.

(ii) The effect of *finite* amplitudes on the period of a vibrating *inviscid* jet in the absence of gravity is calculated by computing the corrections to Rayleigh's two-dimensional result (3.2) up to $O(\delta^2)$, which is necessary to capture the first frequency correction:

$$\omega^2 = \frac{6\sigma}{\rho a_0^3}\left(1 - \frac{37}{24}\frac{\delta^2}{a_0^2}\right) + o(\delta^2), \tag{3.5}$$

where δ is the amplitude of perturbation about the mean radius a_0.

(iii) To account for the free surface curvature in the axial direction, Bohr notes Rayleigh's (1879) dispersion relation,

$$\omega^2 = \frac{\sigma i a_0 k J_2'(i a_0 k)}{\rho J_2(i a_0 k) a_0^3}(3 + a_0^2 k^2), \tag{3.6}$$

for infinitely small oscillations of an inviscid jet in three dimensions. This expression follows from assuming a free surface of the form:

$$r(\theta, z, t) = a_0(1 + \delta \cos n\theta \cos kz \cos \omega t + O(\delta^2)), \tag{3.7}$$

and again setting $n = 2$ to approximate an ellipse.

Bohr posited a combination of the above three disparate analyses together with Rayleigh's relation (3.3) and proposed the following phenomenological expression for surface tension:

$$\sigma = \frac{k^2 \rho a_0^3 v^2 J_2(i a_0 k)}{i a_0 k J_2'(i a_0 k)(3 + a_0^2 k^2)}\left(1 + \frac{37}{24}\frac{\delta^2}{a_0^2}\right)\left[1 + 2\left(\frac{2\mu}{\rho v a_0^2 k}\right)^{3/2} + 3\left(\frac{2\mu}{\rho v a_0^2 k}\right)^2\right], \tag{3.8}$$

where

$$k = 2\pi/\lambda \tag{3.9}$$

is the wavenumber of the free surface oscillation, v is the axial velocity of the jet, given by the ratio of the volumetric flow rate q and the cross-sectional area A,

$$v = \frac{q}{A} = \frac{q}{\pi a_0^2}, \tag{3.10}$$

and ρ and μ are the density and shear viscosity, respectively, of the fluid (assumed known). The amplitude δ of the perturbation and the mean radius a_0 of the jet are deduced from the measured maximal dimension $2R_{max}$ and minimal dimension $2R_{min}$ of the oscillating free surface jet profile from the relations

$$\delta = \tfrac{1}{2}(R_{max} - R_{min}), \tag{3.11}$$

$$a_0(1 + \delta^2/6a_0^2) = \tfrac{1}{2}(R_{max} + R_{min}). \tag{3.12}$$

Note that Bohr assumes a superposition of disconnected results from three different analyses, one linear, two-dimensional, and weakly viscous, another nonlinear inviscid and two-dimensional, and the third linear, inviscid, and three-dimensional. Expression (3.8) therefore should be viewed as *ad hoc*, but nonetheless it has been used satisfactorily to the present day (Caskey & Barlage 1971; Defay & Hommelen 1958; Hansen *et al.* 1958; Kochurova & Rusanov 1981; Rideal & Sutherland 1952; Thomas & Potter 1975; Bleys & Joos 1983; Lukenheimer, Serrien & Joos 1990; Joos & Serrien 1989; Zhang & Zhao 1989).

In the practical application of Bohr's model there is an ambiguity as to which measurements should be selected as R_{max} and R_{min}, as we now explain.

We define the maximum dimensions of the jet cross-section at the beginning, middle, and end of the wavelength to be $2R^B_{max}$, $2R^M_{max}$, and $2R^E_{max}$, respectively, and the minimum dimensions to be $2R^B_{min}$, $2R^M_{min}$, and $2R^E_{min}$ (see figure 2). In Bohr's model, the axial velocity of the jet and the amplitude and wavelength of the free surface oscillation are constant along the jet axis. This follows from the neglect of gravity and the fact that viscosity is only added *a posteriori*. Referring to figure 2, the Bohr model therefore assumes

$$\begin{aligned} R^B_{max} &= R^M_{max} = R^E_{max}, \\ R^B_{min} &= R^M_{min} = R^E_{min}. \end{aligned}$$

However, all jets that we measured satisfy

$$\begin{aligned} R^B_{max} &> R^M_{max} > R^E_{max}, \\ R^B_{min} &\neq R^M_{min} \neq R^E_{min}. \end{aligned}$$

The fact that R_{max} and R_{min} are not uniform down the jet indicates that in all physical jets, even those with small dimensions, high velocities, and low viscosities, the effects of gravity and viscosity are measureable. The effect of gravity is to decrease R_{max} and R_{min} from one wavelength to the next; the effect of viscosity is to decrease R_{max} and increase R_{min}.

In the Bohr model, it is just as valid to take $(R_{max}, R_{min}) = (R^B_{max}, R^M_{min})$ or (R^E_{max}, R^M_{min}) or $(\frac{1}{2}(R^B_{max} + R^E_{max}), R^M_{min})$ or $(R^M_{max}, \frac{1}{2}(R^B_{min} + R^E_{min}))$, etc. But, as a practical matter, these choices result in different values of a_0 and δ for equation (3.8), and produce different values for surface tension σ (we give the percentage difference in a particular example in §5). As stated earlier, Rayleigh's and Bohr's analyses neglect gravity. Geer &

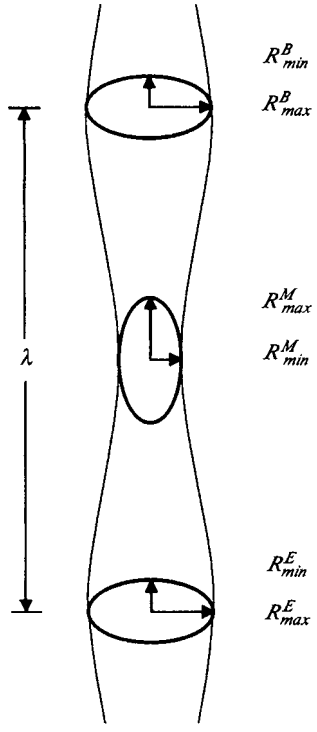

FIGURE 2. Measurements taken of the oscillating jet.

Strikwerda (1983) and Keller (1983) generalize this analysis to include the acceleration due to gravity; their extension has not been exploited for determining surface tension to our knowledge.

3.3. *Recent oscillating jet applications and alternative techniques*

We now briefly review various modifications of Bohr's relation (3.8) which have been applied in combination with oscillating jet measurements to determine dynamic surface tension. We then note alternative methods in the literature.

Defay & Hommelen (1958) suggested a simplified form of (3.8),

$$\sigma = \frac{2\rho q^2}{3a_0\lambda^2 + 5\pi^2 a_0^3}\left(1 + \frac{37}{24}\frac{\delta^2}{a_0^2}\right), \tag{3.13}$$

which follows from Bohr's relation if viscosity is neglected and one retains the leading-order terms in a small argument expansion of the Bessel functions. The authors contend that this formula is useful for low-viscosity liquids. Kochurova & Rusanov (1981) proposed a further modification of (3.13),

$$\sigma = \frac{4q^2 K(\rho 1 + \rho_2)}{6a_0\lambda^2 + 10\pi^2 a_0^3}\left(1 + \frac{37}{24}\frac{\delta^2}{a_0^2}\right), \tag{3.14}$$

where K is an arbitrary constant obtained from experimental data and ρ_1, ρ_2 are the densities of the fluid and ambient atmosphere, respectively.

Alternative techniques employed to determine dynamic surface tension include the following.

(i) The maximum bubble pressure technique has been widely used (Bendure 1971; Garret & Ward 1988; Kao *et al.* 1991; Edwards *et al.* 1991) to determine the dynamic

surface tension of new surfaces. In this technique a flow of gas into a reservoir of the test liquid produces a stream of bubbles; the surface tension of the gas/liquid interface is deduced from measurements of the maximum pressure in each bubble before it detaches into the liquid. There are drawbacks of the maximum bubble pressure technique with regard to the millisecond timescale measurements relevant for spinning and spraying processes. First, the stream of bubbles is limited to a rate of about ten bubbles per second in water and fifteen bubbles per second in alcohol, which yields measurements for a surface age of several hundreths of a second. Second, the bubble pressure technique is calibrated against two known systems, typically pure water/nitrogen and alcohol/nitrogen, from which the technique interpolates all other interfaces. Extrapolation of this technique to fundamentally different materials is speculative.

(ii) The Langmuir trough method (Langmuir 1917; Edwards *et al.* 1991) is used to determine the dynamic surface tension of newly created monolayers.

(iii) The falling meniscus method and the pulse drop method (Edwards *et al.* 1991) are employed to determine the dynamic surface tension for surfaces that are initially deformed and gradually return to their equilibrium state.

All of the methods listed above are best suited for purposes distinct from spray and spinning applications.

4. An alternative model for dynamic surface tension measurements; extension to the measurement of elongational viscosity

Recall from §3 that the classical inverse models of Rayleigh and Bohr consist of explicit formulae for surface tension which are combined with experimental measurements. Here we provide further resolution in the inverse model by not insisting on a closed-form analytical expression for surface tension (or other material parameters). Rather, we derive models in the form of coupled differential equations from the full three-dimensional boundary value problem of §2, with the derivation based on flow assumptions that can be independently tested. With current computational capabilities, inverse codes which iterate on systems of ordinary differential equations to deduce surface tension or other material coefficients in the model are tractable and inexpensive. By admitting models in the form of systems of steady differential equations, the methods of the present paper are proposed as a platform not just for higher resolution of surface tension, but also for further material characterization.

In this section we first list and discuss all assumptions upon which our model is based. We then summarize our numerical tests (Petersson 1994) and related studies of the fundamental geometric assumption that the free surface cross-section remains elliptical in a surface-tension-dominated flow. Because of difficulties with numerical methods for the three-dimensional free surface problem, we thus far are only able to test the critical assumptions for the idealized inviscid, transverse two-dimensional free surface equations without gravity. We also recall relevant results of similar studies assuming weak viscosity without gravity (Mansour & Lundgren 1990) and inviscid jets with gravity (Geer & Strikwerda 1983). Finally, we present our steady integro-differential equation model which is derived from the full three-dimensional free surface boundary value problem based on these assumptions.

4.1. *Assumptions to simplify the three-dimensional boundary value problem*

To derive our model, we make the following assumptions.

(*a*) The jet is slender, defined in terms of a slenderness ratio ε,

$$0 < \varepsilon = r_0/z_0 \ll 1, \tag{4.1}$$

where r_0 is a characteristic length scale in the cross-sectional plane coordinatized by x_1 and x_2 (e.g. the maximum mean radius of the jet over the domain of measurements), and z_0 is a characteristic length scale in the axial, or x_3, direction (e.g. the minimum wavelength of oscillation in the axial direction).

(*b*) The flow is steady. (This is not essential; refer to Bechtel, Forest & Lin 1992*b*; Bechtel *et al.* 1988 for transient forms of various slender jet models.)

(*c*) The fluid is viscous, *but not necessarily Newtonian.*

(*d*) The fluid density is constant along the wavelength over which measurements are taken. *The surface tension and viscosity do not have to be constant.*

(*e*) The velocity in the axial, or x_3, direction is assumed to be of the form

$$v_3 = v_0[v(x_3) + O(\varepsilon^2)], \tag{4.2}$$

where v_0 is a characteristic axial velocity and $v(x_3)$ is a dimensionless $O(1)$ function of the axial coordinate x_3.

(*f*) The velocity components in the x_1 and x_2 directions are of the form

$$v_1 = v_0[(x_1/z_0)\zeta_1(x_3) + O(\varepsilon^2)], \tag{4.3}$$

$$v_2 = v_0[(x_2/z_0)\zeta_2(x_3) + O(\varepsilon^2)], \tag{4.4}$$

where $\zeta_1(x_3)$ and $\zeta_2(x_3)$ are dimensionless $O(1)$ functions of the axial coordinate x_3.

(*g*) The jet exits an elliptical orifice and its cross-section remains elliptical for the distance over which measurements are taken. The free surface therefore can be represented by

$$f(x_1, x_2, x_3) = \frac{x_1^2}{\Phi_1^2(x_3)} + \frac{x_2^2}{\Phi_2^2(x_3)} - 1 = 0, \tag{4.5}$$

where $\Phi_1(x_3)$ and $\Phi_2(x_3)$ are the semiaxes of the cross-section at the axial location x_3.

Assumptions (*a*) and (*b*) are dictated by the experimental design. Importantly, our small parameter ε is based on the transverse-to-downstream aspect ratio of the oscillating jet, as opposed to the amplitude of oscillation in Rayleigh's and Bohr's analyses. Thus, our model is a slender asymptotic approximation which yields a fully nonlinear leading-order system, whereas previous analyses of Bohr and Rayleigh involve linearization at leading order.

Assumptions (*a*), (*e*), (*f*), and (*g*) are the backbone of a systematic and comprehensive perturbation theory for slender jets (Bechtel *et al.* 1992*a*, *b*). Given these assumptions one can rigorously derive self-consistent one-dimensional models (closed sets of one-dimensional equations at each order in the perturbation expansion) for slender jets. Moreover, the modelling is general enough to capture experimental and physical effects which are either inescapable (such as gravity) or desirable (a rheology more complicated than Newtonian viscosity, thermal effects, non-constant density, etc.), none of which are included in the classical models.

Assumption (*g*) generalizes Rayleigh's and Bohr's assumption that the departure of the cross-section from circular is small. Our assumption is more practical for physical experiments, since the departure of the oscillation from a circular cross-section must be sufficient for discernible measurements of wavelength and amplitude,

and high-frequency capillary waves that are troublesome numerically would be hard to distinguish from the physical oscillations. In the absence of surface tension, an elliptical inviscid free surface flow is an exact solution of the three-dimensional free-surface b.v.p. (Geer & Strikwerda 1983; Tuck 1976). In the presence of surface tension, the ellipse distorts downstream. The evidence, both experimental and numerical, is that for moderate eccentricities (2.5:1 or less) the elliptical shape remains nearly elliptical for at least a few wavelengths of oscillation. We expand on this issue when our numerical tests are presented.

Assumptions (*c*), (*d*) and (*e*) allow for more general flows than the Rayleigh and Bohr models. In particular, assumption (*e*) is equivalent to Rayleigh's and Bohr's assumption that the motion within the jet cross-section is two-dimensional, but we have generalized Rayleigh and Bohr's analyses by allowing the axial velocity to be a function of axial coordinate x_3. The classical models assume the axial velocity is constant to leading order, but we allow acceleration downstream. All experiments, as well as our analysis, demand this generalization, *which is essential to incorporate the effects of gravity and surface tension gradients.* Rayleigh's and Bohr's appropriation of two-dimensional oscillating cylinder solutions to the three-dimensional oscillating jet problem of figure 1 through the identification (3.3) makes sense only if the jet axial velocity is constant. Our asymptotic methods *deduce*, for slender jets, a direct correspondence between the two-dimensional oscillating cylinder problem and the flow of figure 1. In the special case of no gravity and constant surface tension we deduce relation (3.3).

The primary assumptions in our model are that the initial elliptical jet cross-section remains elliptical at least through one oscillation and that the jet is slender, which replace Rayleigh's and Bohr's assumption that the departure of the cross-section from circular is small. Previous numerical studies have explored the evolution of an initially elliptical cross-section under similar assumptions. Geer & Strikwerda (1983) studied, among other issues, how an elliptical cross-section distorts under the influence of gravity and surface tension.

Petersson (1994) re-examines the validity of our assumptions in numerical simulations of a idealized inviscid two-dimensional flow with surface tension and without gravity, utilizing current numerical techniques (Baker, Meiron & Orszag 1982; Mansour & Lundgren 1990; Lundgren & Mansour 1988; Hou, Lowengrub & Krasny 1991). We consider this study of the idealized inviscid case as a quantitative test of the loss of accuracy which follows from our assumption (*g*) that the initial elliptical jet cross-section remains elliptical at least through one oscillation. Since surface tension and inertia are the dominant effects distorting the elliptical shape, we do not anticipate that these tests will differ significantly once we are able to numerically couple viscosity and gravity. The conclusions of Petersson (1994) are summarized below:

Figure 3 depicts the variation of the shape of the cross-section when the initial aspect ratio is 1.5. Note that the cross-section remains nearly elliptical for the complete period shown.

In figure 4 we compare the free surface semiaxis $\phi_1(t)$ (the dimensionless form of $\Phi_1(t)$ defined ahead in equation (4.7)) from the inviscid 2-dimensional numerical computation to the Lagrangian representation $\phi_1(t)$ of the free surface semiaxis from the special case of our oscillating jet model with the effects of gravity and viscosity suppressed for the comparison. The only direct problem that Bohr solves where the free surface profile is deduced from known material properties is the inviscid problem without gravity; in figure 4 we also display Bohr's corresponding solutions, and note

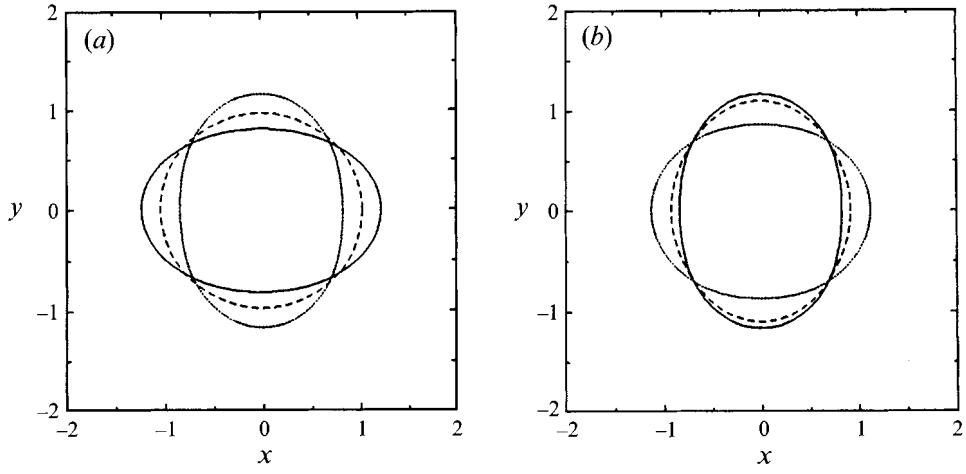

FIGURE 3. The deformation of the cross-section with initial aspect ratio 1.5 during the first oscillation, from the two-dimensional inviscid numerical simulations of Petersson (1994). (*a*) The cross-section at times 0.0 (solid), 0.603 (dashed) and 1.072 (dotted); (*b*) times 1.072 (solid), 1.781 (dashed) and 2.254 (dotted).

that they are very close to the solutions from our theory. We re-emphasize, however, that a primary advantage of our model over the Bohr model is that our model deduces the effects of gravity and viscosity self-consistently from the three-dimensional physics.

From figure 4 we observe that our one-dimensional model underestimates the first period of oscillation, by less than 0.5% in the 1.5 aspect ratio case and 2.0% in the 2.0 aspect ratio case. These discrepancies would translate in the inverse problem into errors of 1.0% and 3.5%, respectively, in predictions of the surface tension.

We infer from these tests that for oscillating jets with aspect ratio 2.0 our model is capable of quantitative accuracy with errors in predicted wavelength on the order of 2.0%, which translates in the inverse problem to surface tension measurements with an error on the order of 3.5%.

4.2. *Our model for the oscillating jet with viscosity and gravity: the direct problem*

We now exploit our assumptions outlined in § 4.1 to reduce the 3-dimensional free surface b.v.p. to a scalar 1-dimensional equation, following Bechtel *et al.* (1988). We first non-dimensionalize the problem by scaling all quantities by the characteristic velocity v_0, characteristic axial length z_0, and characteristic transverse length r_0. In particular we define the dimensionless coordinates x, y, z through

$$x = x_1/r_0, \quad y = x_2/r_0, \quad z = x_3/z_0, \tag{4.6}$$

and the dimensionless semiaxes of the elliptical jet cross-section through

$$\phi_1(z) = \frac{\Phi_1(x_3)}{r_0} \quad , \quad \phi_2(z) = \frac{\Phi_2(x_3)}{r_0}. \tag{4.7}$$

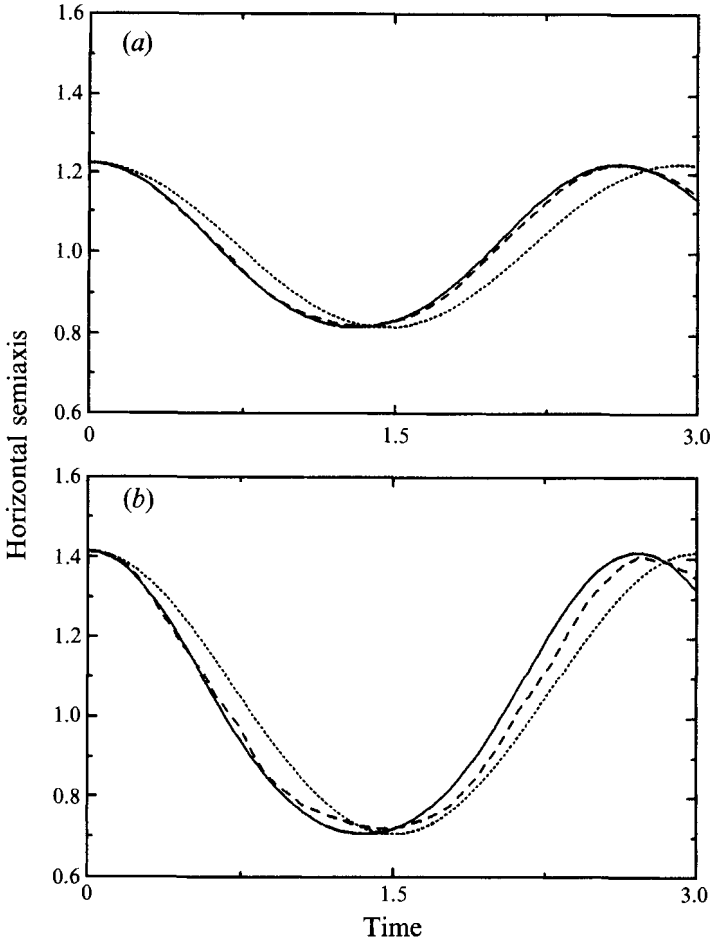

FIGURE 4. The free surface semiaxis $\phi_1(t)$ as function of time for initial aspect ratios 1.5 (*a*) and 2.0 (*b*). The solid lines are the solutions from the asymptotic theory developed ahead in § 4.2 with the effects of gravity and viscosity suppressed for the purpose of comparison to the numerical solutions. The dotted lines are the solutions from Bohr's forward problem, which neglects gravity and viscosity. The dashed lines are $\phi_1(t)$ from the two-dimensional inviscid numerical solutions of Petersson 1994.

Assumptions (*a*), (*e*), and (*f*) of § 4.1 and the non-dimensionalization (4.6) imply a rate of strain tensor of the form

$$\boldsymbol{D} = \begin{bmatrix} (v_0/z_0)\zeta_1 & 0 & \varepsilon(v_0/z_0)x\zeta_{1,z} \\ 0 & (v_0/z_0)\zeta_2 & \varepsilon(v_0/z_0)y\zeta_{2,z} \\ \varepsilon(v_0/z_0)x\zeta_{1,z} & \varepsilon(v_0/z_0)y\zeta_{2,z} & (v_0/z_0)v_{,z} \end{bmatrix} + O(\varepsilon^2), \tag{4.8}$$

so that $\boldsymbol{D}$ is diagonal to leading order in ε, and hence the oscillating jet flow is *elongational to leading order*. This flow is the elliptical transverse generalization of von Kármán's (1921) axisymmetric plug flow ansatz which he used to study unbounded steady flow induced by an infinite, uniformly rotating planar disc.

We select the origin $z = 0$ to be the beginning of the wavelength (refer to figure 2). We choose the characteristic velocity v_0 to be the axial velocity v_3 at this origin,

$$v_0 = v_3(0), \tag{4.9}$$

and the characteristic transverse scale r_0 to be the geometric mean of the elliptic semi-axes at $z = 0$,

$$r_0 = [\Phi_1(0)\Phi_2(0)]^{1/2} = (R^B_{max}R^B_{min})^{1/2}. \tag{4.10}$$

We postpone selection of the axial length scale z_0 until just after equation (4.24).

The three-dimensional problem is reduced to one dimension in the slender asymptotic limit by

(i) multiplying the x-component of the momentum equation (2.4) by x and integrating over the jet cross-section,

(ii) multiplying the y-component of the momentum equation (2.4) by y and integrating over the jet cross-section,

(iii) integrating the z-component of momentum equation (2.4) over the jet cross-section,

(iv) retaining only the leading-order terms in the slenderness ratio $\varepsilon = r_0/z_0$,

(v) using the kinetic free surface boundary condition (2.7) to replace the boundary terms of velocity and pressure, that appear through the divergence theorem in these integrations, with surface tension and ambient pressure terms.

We then use incompressibility (2.3), the kinematic free surface boundary condition (2.5), and the z-component of the momentum equation to eliminate ζ_1, ζ_2, ϕ_2, and v.

If the surface tension σ varies along the perimeter of the cross-section and along the length of the jet, i.e. $\sigma = \sigma(x_s, y_s, z)$ where x_s and y_s are points on the surface of the jet cross-section, *and* all possible terms incorporated in the model are important in the leading order competition between physical effects, then the reduction outlined above results in

$$[1+\phi_1^4 v]\phi_{1,zz} - 2\frac{\phi_{1z}^2}{\phi_1} + 4\phi_1^3(\Psi_s - \Psi_c) + \frac{1}{F}[\phi_1^4 - v^{-1}]\phi_{1,z}$$

$$+ \oint \frac{1}{W\sigma}\left(x_s\frac{\partial\sigma}{\partial x_s} - y_s\frac{\partial\sigma}{\partial y_s}\right)\mathrm{d}u - \frac{2}{F^2}v^{-2}\phi_1 + \frac{48}{R}v^{-1/2}\phi_1^2\left[v\phi_{1,z} + \frac{\phi_1}{2F}\right] = 0, \tag{4.11}$$

$$vv_{,z} = \varepsilon^2\left(G(z)v_{,z} - \frac{1}{\pi\phi_1\phi_2}S(z)\right) + \frac{1}{F}, \tag{4.12}$$

$$\phi_2(z) = [v(z)\phi_1(z)]^{-1}, \tag{4.13}$$

where

$$\Psi_c = \Psi_c(z) = \frac{-\phi_1\phi_2}{\pi}\int_0^{2\pi}\frac{1}{W}\frac{\cos^2\theta\,\mathrm{d}\theta}{(\phi_1^2\sin^2\theta + \phi_2^2\cos^2\theta)^{3/2}}, \tag{4.14}$$

$$\Psi_s = \Psi_s(z) = \frac{-\phi_1\phi_2}{\pi}\int_0^{2\pi}\frac{1}{W}\frac{\sin^2\theta\,\mathrm{d}\theta}{(\phi_1^2\sin^2\theta + \phi_2^2\cos^2\theta)^{3/2}}. \tag{4.15}$$

The notation $\oint f(x_s(u,z), y_s(u,z), z)\mathrm{d}u$ indicates the line integral of f evaluated on the free surface, around the cross-section; said differently, the surface is parameterized by the axial coordinate z and a transverse coordinate u, and f is integrated over u at fixed z. The solution of (4.11)–(4.13) gives the dimensionless cross-sectional semiaxes $\phi_1(z)$ and $\phi_2(z)$ and the axial velocity $v(z)$ of the jet as functions of the dimensionless axial coordinate z. The integration constants in (4.11), (4.12), and (4.13) are determined by our choices (4.9) and (4.10) for the characteristic scales v_0 and r_0. All material

properties and characteristic scales are contained in the dimensionless parameters

$$\left.\begin{aligned} W &= W(x_s, y_s, z) = \frac{\rho r_0^3 v_0^2}{\sigma(x_s, y_s, z) z_0^2}, \quad F = \frac{v_0^2}{g z_0}, \quad G(z) = \frac{(\partial\eta/\partial z) z_0}{\rho v_0 r_0^2}, \\ R(z) &= \frac{\rho r_0^2 v_0}{\eta(z) z_0}, \quad S(z) = \frac{z_0^2}{\rho v_0^2 r_0^3} \int_0^{2\pi} \left(\oint \frac{\partial \sigma}{\partial z} \mathrm{d}u \right). \end{aligned}\right\} \tag{4.16}$$

The Froude number F is a constant; the Weber number $W(x_s, y_s, z)$ is a function of all spatial coordinates on the free surface, since surface tension $\sigma(x_s, y_s, z)$ is allowed to vary along the length and around the cross section of the free surface. The function $S(z)$ indicates the relative importance of the axial gradient of surface tension along the jet. In its primitive form, the elongational viscosity η depends upon the three invariants of the rate of strain tensor $\boldsymbol{D}$, namely I_D, II_D, and III_D. The incompressibility condition reduces I_D to zero. In a slender jet flow the other two invariants are to leading order functions of z only, as can be seen from equation (4.6). Therefore, in our leading-order model the effective viscosity (and hence the Reynolds number R) is a function of z only.

Note that we have retained $O(\varepsilon^2)$ terms in equation (4.12), whereas all other terms appear to be dominant and $O(1)$. The $O(\varepsilon^2)$ terms represent the possible coupling of axial variations in viscosity and surface tension through the integrated axial momentum equation, which would occur only if $G(z)$ and/or $S(z)$ are $O(\varepsilon^{-2})$ or larger.

In the direct problem given by equations (4.11), (4.12), and (4.13) the surface tension and viscosity, and hence W, S, and R, are specified functions of position. For example, it may be assumed that in the presence of dilute surfactants the variation of surface tension is given by a Gibbs equation of state (Adamson 1982; Rosen 1988)

$$\sigma_s - \sigma = \Gamma^* \bar{R} T, \tag{4.17}$$

where σ_s and σ are the surface tensions of the uncontaminated and actual surfaces respectively, Γ^* is the surface concentration of the surfactant, $\bar{R}$ is the gas constant, and T is the absolute temperature. Other equations giving explicit relationships between σ and σ_s may be found in Edwards *et al.* (1991); Borwanker & Wasan (1983); Stone & Leal (1990); Lin, McKeigue & Maldarelli (1990); Milliken *et al.* (1993). In addition to a constitutive assumption on σ such as (4.17), one also couples a surfactant mass transport equation (Probstein 1989; Stone & Leal 1990; Edwards *et al.* 1991; Swean & Beris 1994).

In this paper, we pursue physical situations where $G(z)$ and $S(z)$ are $O(1)$ or less. This reduces (4.12) to a form which integrates exactly to

$$v(z) = \left(\frac{2z}{F} + 1 \right)^{1/2}, \tag{4.18}$$

the standard axial velocity profile (Geer 1977; Petrie 1979) of a cylindrical jet falling under gravity. If the change in surface tension is a function only of the time of exposure τ of the surface to ambient conditions, i.e. the age of the newly formed surface, then in our steady Eulerian formulation $\sigma = \bar{\sigma}(z)$. Explicitly, if $S(z)$ is $O(1)$ or less then, from (4.18), the dimensionless age τ of the surface from $z = 0$ is

$$\tau(z) = \int_0^z \frac{\mathrm{d}\tilde{z}}{v(\tilde{z})} = F \left(\frac{2z}{F} + 1 \right)^{1/2} - 1, \tag{4.19}$$

so that if the variation $\sigma(\tau)$ of surface tension with age is known, it may be converted

to a function of z through

$$\sigma = \tilde{\sigma}(\tau) = \tilde{\sigma}\left(F\left(\frac{2z}{F}+1\right)^{1/2} - 1\right) = \bar{\sigma}(z). \tag{4.20}$$

For the balance of physical effects where $S(z)$ is not leading order, and when $\sigma = \sigma(z)$, the leading-order oscillating jet model consists of equations (4.13), (4.18), and

$$\left[1+\phi_1^4\left(\frac{2z}{F}+1\right)\right]\phi_{1,zz} - 2\frac{\phi_{1z}^2}{\phi_1} + \frac{4}{W}\phi_1^3(\psi_s - \psi_c) + \frac{1}{F}\left[\phi_1^4 - \left(\frac{2z}{F}+1\right)^{-1}\right]\phi_{1,z}$$

$$-\frac{2}{F^2}\left(\frac{2z}{F}+1\right)^{-2}\phi_1 + \frac{48}{R}\left(\frac{2z}{F}+1\right)^{-1/2}\phi_1^2\left[\left(\frac{2z}{F}+1\right)\phi_{1,z} + \frac{\phi_1}{2F}\right] = 0, \tag{4.21}$$

where the dimensionless parameter F is defined in equation (4.16) while W and R are now given by

$$W = \frac{\rho r_0^3 v_0^2}{\sigma(z) z_0^2}\,, \quad R = \frac{\rho r_0^2 v_0}{\eta(z) z_0}. \tag{4.22}$$

The surface curvature effects appear through the elliptic-integral expressions

$$\psi_c = \psi_c(z) = \frac{-\phi_1\phi_2}{\pi}\int_0^{2\pi} \frac{\cos^2\theta\,\mathrm{d}\theta}{(\phi_1^2\sin^2\theta + \phi_2^2\cos^2\theta)^{3/2}}, \tag{4.23}$$

$$\psi_s = \psi_s(z) = \frac{-\phi_1\phi_2}{\pi}\int_0^{2\pi} \frac{\sin^2\theta\,\mathrm{d}\theta}{(\phi_1^2\sin^2\theta + \phi_2^2\cos^2\theta)^{3/2}}. \tag{4.24}$$

Recall from equations (4.2)–(4.3), (4.7), (4.8) that our theory demands three characteristic scales, namely a transverse length scale r_0, an axial length scale z_0, and an axial velocity scale v_0. Definitions (4.9) and (4.10) explicitly select r_0 and v_0. The obvious choice for the final characteristic scale z_0 is the wavelength of oscillation, but it is *a priori* unknown. We therefore select z_0 to be a reasonable guess for the wavelength, say ten times the initial mean radius r_0. The prescience of this choice is not important, due to a scale invariance property of the leading-order differential equations, (4.11), (4.12), (4.13), or (4.21), (4.18), (4.13). Namely, if z_0 is replaced by az_0 then the dimensionless parameters satisfy $W(az_0) = W(z_0)/a^2, F(az_0) = F(z_0)/a, G(a_0z_0) = G(z_0), R(az_0) = R(z_0)/a, S(az_0) = aS(z_0)$. It follows that if the axial coordinate z is replaced by z/a and the scale z_0 by az_0, then the leading-order equations are invariant. The significance of this property is that the *dimensional* solution is independent of z_0. For example, if we choose $z_0 = 10r_0$ in our model and compute a dimensionless wavelength $\lambda = 1.8$, then the choice of $z_0 = 20r_0$ would yield a dimensionless wavelength $\lambda = 0.9$. For either choice, the *dimensional* wavelength is $18r_0$.

The dimensionless direct (forward) problem in a particular regime consists of solving the governing differential equations ((4.11), (4.12) and (4.13), or (4.21), (4.18) and (4.13)) for specified surface tension and viscosity functions, and specified conditions at $z = 0$, to obtain the values of the jet response $\phi_1(z)$ along the length of the jet, $z > 0$. The dimensional solution is then produced by multiplying by the characteristic length and velocity scales as indicated in equations (4.2)–(4.3), (4.7), (4.8). Figure 5 shows the effect of viscosity and gravity in the regime of equations (4.21), (4.18), and (4.13) on the dimensional jet profile for a water jet with flow rate 45 g s^{-1} from an elliptical orifice with major axis 0.6 cm and minor axis 0.3 cm. Note that viscosity and gravity each have a significant effect on both the amplitude and wavelength of

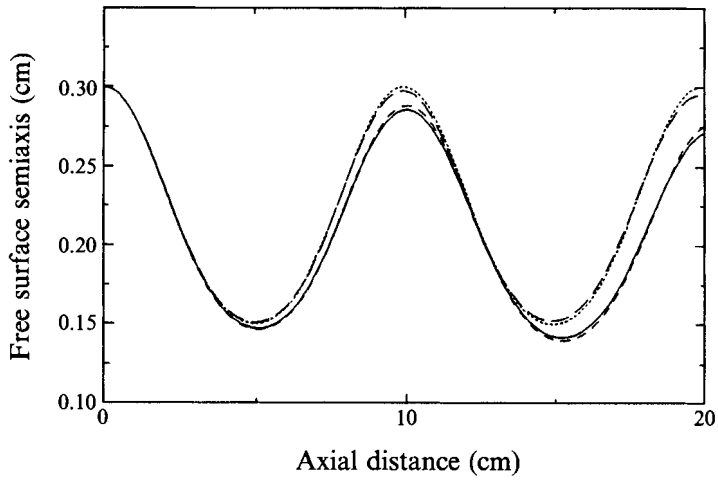

FIGURE 5. The effect of viscosity and gravity on an oscillating water jet (density = 0.9974 g cm^{-3}, elongational viscosity = 3.015 cP) into air (surface tension = 72.03 dyn cm^{-1}, acceleration due to gravity = 981 cm s^{-2}) with flow rate 45 g s^{-1} from a 0.6 × 0.3 cm elliptical orifice. The free surface profile predicted by our model (4.21) neglecting gravity and viscosity: $W = 2.992, 1/R = 1/F = 0$ (dotted); neglecting gravity but including viscosity: $W = 2.992, R = 655.6, 1/F = 0$ (long dashed); neglecting viscosity but including gravity: $W = 2.992, 1/R = 0, F = 48.94$ (dashed); and including gravity and viscosity: $W = 2.992, R = 655.6, F = 48.94$ (solid).

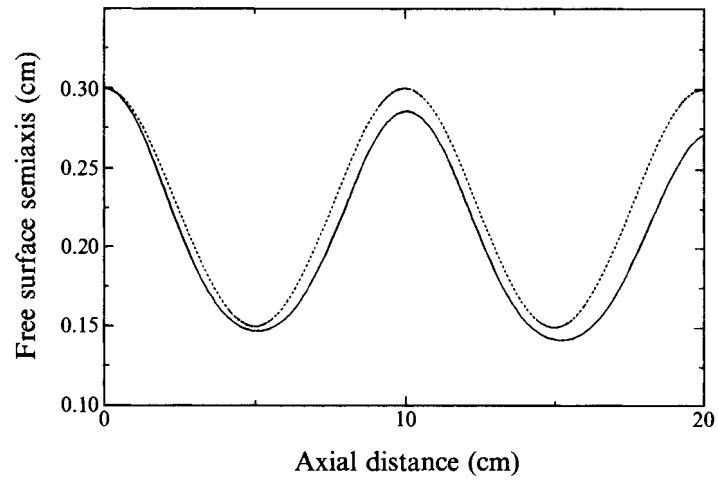

FIGURE 6. Comparison of the predictions of Bohr's and our direct models for the oscillating jet of figure 5. Our prediction including gravity and viscosity: $W = 2.992, R = 655.6, F = 48.94$ (solid); Bohr's prediction, which does not include gravity and viscosity: $W = 2.992$ (dotted). (While Bohr's inverse formula includes viscosity his direct model does not.)

the oscillating jet profile. Our experience indicates these effects are always measurable and therefore *should* be included in any model which seeks to adequately characterize material properties based on measurements of oscillating jets. Figure 6 compares jet profiles predicted by Bohr's model and our model (4.21) for the oscillating jet of figure 5. The direct problem is studied in Bechtel (1989).

4.3. *The inverse problem*

For our application to material characterization we must solve the inverse formulation of our model, i.e. find values of surface tension and viscosity to match specified values of $\phi_1(z)$ at any particular points on the jet profile. The assumption made is that for given functions of Weber number $W(x_s, y_s, z)$, Reynolds number $R(z)$, and Froude number F, and given initial values of ϕ_1, $\phi_{1,z}$ (slope of jet profile) and ϕ_2/ϕ_1 (aspect ratio), there exists a unique jet profile and vice versa. This assumption is confirmed for all examples we have explored.

5. Implementation of the inverse problem

5.1. *The inverse code*

In order to apply the inverse formulation of § 4.3, we perform oscillating jet experiments on ethanol, and from these experiments we deduce the surface tension and viscosity of the fluid. For this test fluid with constant values of surface tension and viscosity, we implement an inverse code based on equations (4.13), (4.18), and (4.21) with W and R constant. The code iterates on the two parameters W and R until the solution of (4.13), (4.18), and (4.21) converges to experimental measurements of the dimensionless wavelength λ^e and amplitude $\phi_1^e(\lambda^e)$ of the jet profile.

The iteration we employ is based on a bisection method in the two parameters. We first guess values of W and R, then iterate on W alone to match the measured wavelength λ^e. Next, bisection on R is applied with fixed W to fit the experimental amplitude $\phi_1^e(\lambda^e)$. We then repeat this procedure until specified tolerances on λ^e and $\phi_1^e(\lambda^e)$ are met. This simple iteration scheme is effective because an increase in W (corresponding to a decrease of surface tension) is accompanied by an increase in the wavelength of oscillation of the jet profile, while an increase in viscosity (a decrease in R) leads to a lessening of the amplitude of vibration.

5.2. *Experimental apparatus and measurements*

The experimental apparatus consists of an air-pressurised reservoir connected to an elliptical-shaped orifice. A Model VC-81D high-resolution video camera (Dage MTI) captures the jet profile and a simultaneous perpendicular view reflected on a mirror inclined at an angle of 45°. The magnification of the camera and lens setup results in digital images on a Princeton Research Model Ultra 16 video monitor (Princeton Graphic Systems) which are approximately 50 times the actual size. Each pair of waveforms is captured with an Epix 16 Meg imaging board (Epix Inc.) and stored on a Bernoulli disk (Iomega). The waveforms are enhanced using an edge detection operation, allowing the coordinates of the edge, accurate to one pixel, to be recorded. Pairs of these coordinates give amplitude and wavelength measurements in pixels. Figure 7 shows the enhanced image of an oscillating water jet; the direct view is on the left and the reflected, perpendicular view is on the right.

Advantages of the current video system are

(*a*) the high-resolution video camera and monitor can produce magnification of 50–200X;

(*b*) computer software allows for identification of individual pixel values; and

(*c*) perpendicular views of the waveform taken simultaneously can be measured.

The current video-based measurement technique combined with the inverse code produces accurate values of surface tension, but a fundamental limitation on transverse resolution inhibits our accuracy for elongational viscosity. Specifically, the

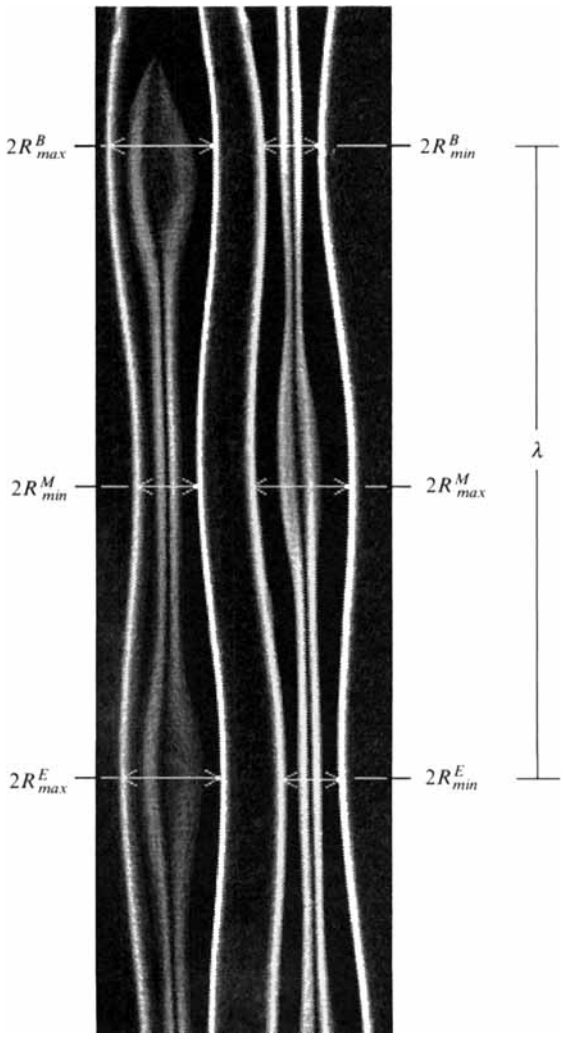

FIGURE 7. Enhanced form of the image of an oscillating water jet.

calculation of surface tension in the inverse code depends primarily on matching the measured wavelength, and an accurate calculation requires a precise measurement of the wavelength of the free surface jet oscillation. The current video system measures wavelengths on the order of 600 pixels, with error bounds of approximately ± 5 pixels. This error is attributable to the small curvature (i.e. flatness) of the oscillating jet profile at its maxima and minima. When combined with the inverse code this precision translates to a variation of approximately $\pm 6\%$ in the calculated surface tension. The resolution of the video system in the transverse direction is typically ± 0.5 pixel on transverse measurement on the order of 60 pixels for the maximum dimensions, and less for the minima. This translates into a limitation on the precision of predictions of elongational viscosity on the order of $\pm 25\%$. Three factors conspire:

(*a*) a complete wavelength of the oscillating jet must be captured on the video screen;

(*b*) the video screen is 1234 pixels in the axial direction $\times$ 1975 pixels in the transverse direction; and

(*c*) the jet is slender.

Even in the best case, where the wavelength takes up the entire 1234 pixel length, the transverse widths of the jet will be on the order of 120 pixels, and so the optimal resolution is ±1 in 120.

Therefore the same feature that works to the advantage of the video system as compared to other image processing techniques becomes a limitation as our analysis pushes the limits of the experimental capability: the inherent digitization of the jet image which allows a rapid analysis of the image using a cursor also imposes a limit on the fineness of transverse resolution.

5.3. *Analysis of the data*

Representative input data obtained from experiments performed on 100% ethanol and output from our inverse code are given in table 1. The raw inputs to the inverse code are:

(i) The wavelength λ and the six maximal and minimal cross-sectional dimensions $2R_{max}$ and $2R_{min}$, respectively, at the beginning, middle, and end of the wavelength (refer to figure 2). In their primitive form these dimensions are taken in pixels from a digitized image on the video screen.

(ii) The density of the liquid, the mass of liquid captured in a time interval while the oscillating jet measurements are being taken, and the duration of the interval. The interval duration is chosen so that the flow rate of the jet is uniform over the interval. The density of the liquid for this particular experiment is a handbook value. The density, mass of liquid, and time of capture are used to calculate volume flow rate and, in conjunction with the area of the cross-section at the beginning of the wavelength $z = 0$, the initial axial velocity $v(0)$.

In addition, five internal values, namely slenderness ratio ε, initial guesses of the Weber number and viscosity, and increments in Weber number and viscosity, are specified for the iteration procedure. Numerical experiments with the inverse code reveal that the predicted values of surface tension and viscosity are independent of these initial guesses, in particular the slenderness ratio, consistent with our earlier discussion that the specific value of z_0 is not important as long as ε is small.

The input data are used to perform the scaling and non-dimensionalization laid out in equations (4.1)–(4.9). The code then inverts the model (given by equations (4.13), (4.18), and (4.21)) to yield output values of surface tension and viscosity and the corresponding Weber and Reynolds numbers. The code has two options in the inversion procedure, max-max and min-min: In the max-max option the code iterates over the wavelength from a maximum to a maximum (R^B_{max} to R^E_{max} in figure 2). For this option the initial conditions on equation (4.21) are

$$\phi_1(0) = \frac{R^B_{max}}{r_0}\ ,\ \phi_{1,z}(0) = 0. \tag{5.1}$$

The code iterates on surface tension and viscosity until it arrives at a solution to equation (4.21) which satisfies, within the specified tolerances,

$$\phi_1(\lambda^e) = \frac{R^E_{max}}{r_0}\ ,\ \phi_{1,z}(\lambda^e) = 0, \tag{5.2}$$

at the dimensionless downstream location

$$\lambda^e = \frac{\lambda}{z_0}. \tag{5.3}$$

	INPUT		
$2 \times R^B_{max}$	63.5	pixels	
$2 \times R^B_{min}$	31.0	pixels	
$2 \times R^M_{max}$	59.5	pixels	
$2 \times R^M_{min}$	33.0	pixels	
$2 \times R^E_{max}$	59.0	pixels	
$2 \times R^E_{min}$	33.5	pixels	
λ^e	593.0	pixels	
horizontal scale	1401.5	pixels cm^{-1}	
vertical scale	1196.5	pixels cm^{-1}	
density	0.7859	g cm^{-3}	
flow rate	0.4011	cm^3 s^{-1}	
	OUTPUT		
code type	max-max	min-min	
surface tension	23.87	23.83	dyn cm^{-1}
elongational viscosity	0.03706	0.04043	g cm^{-1} s^{-1}
checks:			
R^{Mc}_{max}	0.02179	0.02172	cm
R^M_{max}	0.02123	0.02123	cm
%difference	0.6682	0.5833	
R^{Mc}_{min}	0.01149	0.01152	cm
R^M_{min}	0.01177	0.01177	cm
% difference	−0.6177	−0.5307	
R^{Ec}_{min}	0.01188	—	cm
R^E_{min}	0.01195	—	cm
% difference	−0.1478	—	
R^{Ec}_{max}	—	0.02092	cm
R^E_{max}	—	0.02105	cm
% difference	—	−0.1475	

TABLE 1. Input and output data for an oscillating jet of 100% ethanol @ 24 °C

In the min-min option the code iterates from a minimum to a minimum (R^B_{min} to R^E_{min} in figure 2). Table 1 gives the output of the inverse code obtained by running the input data measured in the experiment through the max-max and min-min options. The difference in surface tension is negligible, whereas viscosity varies about 7%.

For comparison, the values of surface tension and shear viscosity in handbooks (Flick 1985; Scheflan & Jacobs 1953), for 100% ethanol at 20° C are 22.2 and 22.3 dyn cm^{-1}, and 1.22 and 1.20 cP respectively. These shear viscosities correspond to elongational viscosities of 3.66 cP and 3.6 cP. The surface tension of the same specimen of 100% ethanol was measured in the same laboratory environment with a DuNouy ring, indicating a value of 22.4 dynes cm^{-1}. These surface tension values are determined from static techniques, and viscosities are measured in shear viscometers, but since ethanol has a constant surface tension and a constant Newtonian viscosity (so that shear viscosity is one third of elongational viscosity), our predictions may be compared. The result of these comparisons for the cases given in table 1 is that our predicted values of surface tension and viscosity agree to within experimental accuracy of the current video system with the handbook values of surface tension and viscosity and the surface tension value obtained with the DuNouy ring. That is,

our predicted surface tension agrees within 7% and the elongational viscosity within 10%, in the worst comparisons.

After giving the output of the inverse problem, namely the viscosity and surface tension, the code then provides some checks of the output. Of the seven length measurements (see figure 2) taken in the experiment, only four are used in the inverse problem: two (R^B_{max} and R^B_{min}) to fix the length scale r_0, and two to iterate on (λ and R^E_{max} in the max-max code, and λ and R^E_{min} in the min-min code). The remaining three measurements (R^M_{max}, R^M_{min}, R^E_{min} in the max-max code, and R^M_{max}, R^M_{min}, R^E_{max} in the min-min code) are not employed in the iteration scheme. As a check the code computes the maxima and minima of the free surface profile corresponding to these three measurements; the degree of agreement between the calculated and measured values is an indication of the accuracy of the model. For the 100% ethanol jet of table 1 the greatest discrepancy is 0.67%.

We also compute values of surface tension from the jet measurements using Bohr's algebraic formula (3.8), with viscosity prescribed to be the handbook value 1.20 cP. Recall that in using Bohr's relation there is ambiguity as to which measurements should be selected as R_{max} and R_{min}. Eight of the possible choices are used to examine the variation of the calculated surface tension due to this selection, and we find the predicted values range from 23.1 to 24.8 dyn cm^{-1}, a spread of 7%. We recall that our model prediction is 23.8 to 23.9 dyn cm^{-1}, which sits in the middle of the Bohr range.

We next apply our inverse code to experiments involving a dilute solution of Nalcotrol in water. Nalcotrol† is an agricultural adjuvant used to change the properties of a pesticide mixture with the intent of producing larger mean droplet sizes in the spray and hence reducing spray drift. The resulting solution is non-Newtonian, and due to the migration of surfactants the tension of a newly formed surface decreases rapidly with time. Although viscosity and surface tension are not constant, the current inverse code predicts an effective viscosity and surface tension over the wavelength (here 0.3 cm) and Lagrangian timescale (here 0.6 ms) in which the measurements are taken. We find that these effective values change with distance downstream of the orifice, as the age of the newly formed surface increases and the deformation rate of the flow decreases.

To more fully exploit the capabilities of our model, which allows η and σ to be non-constant within the wavelength of oscillation, new inverse codes and experiments are required which can then provide information about the variations of viscosity and surface tension on even shorter Lagrangian timescales. This extensive development is underway.

Table 2 contains data from two oscillating jets of Nalcotrol in water at different downstream locations. The surface age of each downstream location is taken to be the age at the middle of the wavelength, and computed using equation (4.19). The second column in table 2 uses data measured between the first and second maxima after the nozzle of an oscillating jet, where the surface is 0.6 ms old while the third column is for data between the third and fourth maxima, where the surface is 1.8 ms old, for two different realizations of the same experiment. Note that the surface tension decreases significantly between these two times, from 111.4 dyn cm^{-1} at 0.6 ms to 84.6 dyn cm^{-1} at 1.8 ms, on its way to an equilibrium static value of 43.2 dyn cm^{-1}

† Reference to a proprietory product is for specific information only, and does not imply approval or recommendation of the product by the The Ohio State University, the US Department of Agriculture, and Los Alamos National Laboratory to the exclusion of others that may be suitable.

	INPUT		
$2 \times R^B_{max}$	62.0	55.0	pixels
$2 \times R^B_{min}$	39.0	44.0	pixels
$2 \times R^M_{max}$	58.0	54.0	pixels
$2 \times R^M_{min}$	42.0	44.0	pixels
$2 \times R^E_{max}$	57.0	54.0	pixels
$2 \times R^E_{min}$	42.0	44.0	pixels
λ^e	401.5	452.0	pixels
horizontal scale	1401.5	1401.5	pixels cm^{-1}
vertical scale	1196.5	1196.5	pixels cm^{-1}
density	0.9976	0.9976	g cm^{-3}
flow rate	0.5648	0.5641	$cm^3 s^{-1}$
	OUTPUT		
code type	max-max	max-max	
surface age	0.5748	1.797	ms
surface tension	111.4	84.63	dyn cm^{-1}
elongational viscosity	18.38	6.169	g cm^{-1} s^{-1}
strain rate	2350	1120	s^{-1}
checks:			
R^{Mc}_{max}	0.02111	0.01944	cm
R^M_{max}	0.02069	0.01927	cm
%difference	0.5085	0.2221	
R^{Mc}_{min}	0.01457	0.01584	cm
R^M_{min}	0.01498	0.01570	cm
% difference	–0.6911	0.2249	
R^{Ec}_{min}	0.01512	0.01597	cm
R^E_{min}	0.01498	0.01570	cm
% difference	0.2242	0.4327	

TABLE 2. Input and output data for two oscillating jets of a 0.05% volume fraction solution of Nalcotrol in water @ 23 °C

measured by the DuNouy ring method. We are not yet sure of the significance of the numerical values beyond their demonstration of a marked decay. It may be, for instance, that the value of 114 dyn cm^{-1} is physical, but it is also likely to be an indication of the limitations of the present inverse model, as discussed above.

The elongational strain rates in the oscillating jet model are the transverse velocity coefficients ζ_1, ζ_2 and axial velocity gradient $v_{,z}$ (see equations (4.2)–(4.4)). In the oscillating jet flow the magnitudes of ζ_1 and ζ_2 are comparable, and both are far greater than the magnitude of $v_{,z}$. For the simulations of table 2 the transverse strain rates have maximum amplitudes of approximately 2350 s^{-1} and 1120 s^{-1}, with corresponding transverse elongational viscosities of 18.37 and 6.17 g cm^{-1} s^{-1}, respectively. Shear viscosities for the Nalcotrol solution measured with a Cannon Manning vacuum viscometer were 7.77 and 3.2 g cm^{-1} s^{-1}, at shear rates of 0 s^{-1} and 21520 s^{-1}, respectively.

6. Summary

We have proposed and applied a combined mathematical model, numerical code and experimental technique for determining elusive material properties of fluids – dynamic surface tension and elongational viscosity. Our surface tension characterization

of a test fluid with constant material properties, 100% ethanol, compares favourably with standard table values and alternative DuNouy ring measurements relevant for static surface tension. As shown by the application to a Nalcotrol agricultural solution, our methodology yields an effective dynamic surface tension of a newly formed surface in an environment consistent with industrial and agricultural applications.

Our techniques further yield an estimate of elongational viscosity, which is likewise an important material property in industrial applications. Limitation in the transverse resolution of our present experimental apparatus prevents us from fully exploiting this capability.

Finally, we mention extensions of this work. As noted at the end of §5, a present focus is on new inverse codes that exploit the model capability to incorporate non-constant surface tension and viscosity, within the wavelength over which measurements are taken. Furthermore, new inverse codes, based on more complicated rheological models, and compatible experiments are being developed to determine additional material properties such as elastic relaxation and temperature-dependent viscosity. Also, we intend to improve transverse resolution of our experimental measurements by recording images on photographic film, which will yield improved accuracy in elongational viscosity measurements.

S. E. Bechtel and M. G. Forest were funded in part by the Air Force Office of Scientific Research under Grants NM90–20253 and F49620–93–1–0431, and the National Science Foundation under Grant CTS-9319128. N. A. Petersson was supported by the US Department of Energy through Los Alamos National Laboratory under contract W–7405–ENG–36. The authors would also like to acknowledge the assistance of Heping Zhu in developing the experimental viscosity apparatus and taking measurements. Finally, the authors acknowledge very constructive input from the referees.

REFERENCES

ADAMSON, A. W. 1982 *Physical Chemistry of Surfaces*, 4th edn. John Wiley & Sons.

BAKER, G. R., MEIRON, D. I. & ORSZAG, S. A. 1982 Generalized vortex methods for free-surface flow problems. *J. Fluid Mech.* **123**, 477–501.

BASARAN, O. A. 1992 Nonlinear oscillations of a viscous liquid drop. *J. Fluid Mech.* **241**, 169–198.

BECHTEL, S. E. 1989 The oscillation of slender elliptical inviscid and Newtonian jets: Effects of surface tension, inertia, viscosity and gravity. *Trans. ASME* E: *J. Appl. Mech.* **56**, 968–974.

BECHTEL, S. E., CAO, J. Z. & FOREST, M. G. 1992*a* Practical application of a higher order perturbation theory for slender viscoselastic jets and fibers. *J. Non-Newtonian Fluid Mech.* **41**, 201–273.

BECHTEL, S. E., FOREST, M. G., HOLM, D. D. & LIN, K. J. 1988 One-dimensional closure models for three-dimensional incompressible viscoelastic free jets: Von Kármán flow geometry and elliptical cross-section. *J. Fluid Mech.* **196**, 241–262.

BECHTEL, S. E., FOREST, M. G. & LIN, K. J. 1992*b* Closure to all orders in 1-D models for slender viscoelastic free jets I. An integrated theory for axisymmetric torsionless flows. *Stability Appl. Anal. Cont. Media* **2**, 59–100.

BENDURE, R. L. 1971 Dynamic surface tension determination with the maximum bubble pressure method. *J. Colloid Interface Sci.* **35**, 238–248.

BLEYS, G. & JOOS, P. 1983 Desorbtion from a slightly soluble monolayer. *Colloid Polymer Sci.* **261**, 1038–1042.

BLEYS, G. & JOOS, P. 1985 Adsorbtion kinetics of Bolaform surfactants at an air/water interface. *J. Phys. Chem.* **89**, 1027–1033.

BOHR, N. 1909 Determination of dynamic surface tension by the method of jet vibration. *Phil. Trans. R. Soc. Lond.* **209**, 281–317.

BORWANKER, R. P. & WASAN, D. T. 1983 The kinetics of adsorbtion of surface-active agents at gas-liquid surfaces. *Chem. Engng Sci.* **38**, 1637–1649.

CASKEY, J. L. & BARLAGE, W. B. 1971 An improved experimental technique for determining dynamic surface tensions of water and surfactant solutions. *J. Colloid Interface Sci.* **35**, 46–52.

CHANG, Y. C., HOU, T. Y., MERRIMAN, B. & OSHER, S. 1995 A level set formulation of Eulerian interface capturing methods for incompressible fluid flows. *J. Comput. Phys.* to appear.

DEFAY, R. & HOMMELEN, J. 1958 Measurements of dynamic surface tensions of aqueos solutions by the oscillating jet method. *J. Colloid Sci.* **13**, 553–564.

EDWARDS, D. A., BRENNER, H. & WASAN, D. T. 1991 *Interfacial Transport Processes and Rheology.* Butterworth-Heinemann.

FLICK, E. W. (ed.) 1985 *Industrial Solvents Handbook* 3rd edn. Park Ridge, New Jersey, USA: Noyes Data Corporation.

GARRET, P. R. & WARD, D. R. 1988 A reexamination of the measurement of dynamic surface tensions using the maximum bubble pressure method. *J. Colloid Interface Sci.* **132**, 475–490.

GEER, J. F. 1977 Slender streams with gravity: Outer asymptotic expansions. I. *Phys. Fluids* **20**, 1613–1621.

GEER, J. F. & STRIKWERDA, J. C. 1983 Vertical slender jets with surface tension. *J. Fluid Mech.* **135**, 155–169.

HANSEN, R. S., PURCHASE, M. E., WALLACE, T. C. & WOODY, R. C. 1958 Extension of the vibrating jet method for surface tension measurements to jets of non-uniform velocity profile. *J. Phys. Chem.* **62**, 210–214.

HOU, T. Y., LOWENGRUB, J. S. & KRASNY, R. 1991 Convergence of a point vortex method for vortex sheets. *SIAM J. Numer. Anal.* **28**, 308–320.

HOU, T. Y., LOWENGRUB, J. S. & SHELLEY, M. J. 1994 Removing stiffness from interfacial flows with surface tension. *J. Comput. Phys.* **114**, 312–338.

JOOS, P. & SERRIEN, G. 1989 Adsorbtion kinetics of lower alkanols at air/water interface: effect of structure makers and structure breakers. *J. Colloid Interface Sci.* **127**, 97–103.

KAO, R. L., EDWARDS, D. A., WASAN, D. T. & CHEN, E. 1991 Measurement of the interfacial dilatational viscosity at high rates of interfacial expansion using the maximum bubble pressure method I. Gas liquid surface. *J. Colloid Interface Sci.* **148**, 247.

KÁRMÁN, T. VON 1921 Über Laminare and Turbulente Reibung. *Z. angew. Math. Mech.* **1**, 233–252.

KELLER, J. B. 1983 Capillary waves on a vertical jet. *J. Fluid Mech.* **135**, 171–173.

KOCHUROVA, N. N. & RUSANOV, A. K. 1981 Dynamic surface tension of water: Surface tension and surface potential. *J. Colloid Interface Sci.* **81**, 297–303.

LANGMUIR, I. 1917 The constitution and fundamental properties of solids and liquids II. Liquids. *J. Am. Chem. Soc.* **39**, 1848–1906.

LIN, S. Y., MCKEIGUE, K. & MALDARELLI, C. 1990 Diffusion-controlled surfactant adsorbtion studied by pendant drop digitization. *AIChE J.* **36**, 1785–1795.

LUKENHEIMER, K., SERRIEN, G. & JOOS, P. 1990 The adsorbtion kinetics of octanol at the air/solution interface measured with the oscillating bubble and the oscillating jet methods. *J. Colloid Interface Sci.* **34**, 407–411.

LUNDGREN, T. S. & MANSOUR, N. N. 1988 Oscillations of drops in zero gravity with weak viscous effects. *J. Fluid Mech.* **194**, 479–510.

MANSOUR, N. N. & LUNDGREN, T. S. 1990 Satellite formation in capillary jet breakup. *Phys. Fluids* A, **2**, 1141–1144.

MILLIKEN, W. J., STONE, H. A. & LEAL, L. G. 1993 The effect of surfactant on the transient motion of Newtonian drops. *Phys. Fluids* A, **5**, 69–79.

PEDERSEN, P. O. 1907 On the surface tension of liquids investigated by the method of jet vibration. *Phil. Trans. R. Soc., Lond.* **207**, 342–397.

PETERSSON, N. A. 1994 Fast numerical computation of 2-D free surface jet flow with surface tension. CAM report 94-32, Department of Mathematics, University of California, Los Angeles. *J. Comput. Phys.* to appear.

PETRIE, C. J. S. 1979 *Elongational flows.* Pitman.

POZRIKIDIS, C. 1992 *Boundary Integral and Singularity Methods for Linearised Viscous Flow.* Cambridge University Press.

PROBSTEIN, R. F. 1989 *Physicochemical Hydrodynamics.* Butterworths.

RAYLEIGH, LORD 1879 On the capillary phenomena of jets. *Proc. R. Soc. Lond.* **29**, 71–97.

RAYLEIGH, LORD 1890 On the tension of recently formed surfaces. *Proc. R. Soc. Lond.* **41**, 281–287.

RIDEAL, E. K. & SUTHERLAND, K. L. 1952 The variations of surface tension of solutions with time. *Trans. Faraday Soc.* **48**, 1109–1123.

ROSEN, M. J. 1988 *Surfactants and Interfacial Phenomena*, 2nd edn. John Wiley & Sons.

SCHEFLAN, L. & JACOBS, M. 1953 *Handbook of Solvents*. D. Van Nostrand Company Inc.

STONE, H. A. & LEAL, L. G. 1990 The effect of surfactants on drop deformation and breakup. *J. Fluid Mech.* **220**, 161–186.

SWEAN, T. F. JR. & BERIS, A. N. 1994 Dynamics of free-surface flows with surfactants. In *Proc. Twelfth US National Congress of Applied Mechanics*. (ed. A. S. Kobayashi), pp. 173–177. ASME

THOMAS, W. D. E. & POTTER, L. 1975 Solution/air interfaces 1. An oscillating jet relative method for determining dynamic surface tension. *J. Colloid Interface Sci.* **50**, 397–412.

TUCK, E. O. 1976 The shape of free jets of water under gravity. *J. Fluid Mech.* **76**, 625–640.

ZHANG, L. H. & ZHAO, G. X. 1989 Dynamic surface tension of the aqueos solutions of cationic-anionic surfactant mixtures. *J. Colloid Interface Sci.* **127**, 353–361.

ZHANG, X., HARRIS, M. T. & BASARAN, O. A. 1994 Measurement of dynamic surface tension by a growing drop technique. *J. Colloid Interface Sci.* **168**, 47–60.